2005-01-2291

# Examination of Clunk Phenomena Using a Non-Linear Torsional Model of a Front Wheel Drive Vehicle with Manual Transmission

**W. Oh and R. Singh**
The Ohio State University



## ABSTRACT

Linear and non-linear simulation models are created to understand, interpret and control the clunk problem in a front-wheel drive vehicle, with focus on tip-in and tip-out induced transients. A reduced order torsional model of the driveline system is employed to conceptually describe the impulsive behavior. Based on the calculated time responses, this investigation attempts to propose a few metrics for the quantification of clunk or sharp transients. The effects of several design parameters, such as the number of gear backlashes and stiffnesses of a two-staged clutch damper, are illustrated. Suggestions for further work and possible design solutions are included.

## INTRODUCTION

The source of sharp "metallic" (or clunk) noise and vibration is typically a sudden change or reversal in the mean torque that excites impacts within torsional sub-systems in many vehicles. Impulsive events may be followed by significant oscillations at the first torsional mode and/or structural resonances of propeller or drive shafts, axles, and housings [1]. Though the literature [1-7] on clunk is sparse, the path seems to be structure-borne as impulses are transferred to the receiver (passenger compartment) via axle, chassis, suspension elements and mounts [2]. Among the earlier studies, Krenz [3] introduced experimental results and identified some empirical design guidelines that could be utilized to reduce the severity of clunk. He had found such methods to be useful in controlling the transient responses, which greatly differ from typical steady state responses within the drivelines. Several recent investigators have used numerical simulations and laboratory tests to better understand such problems [1-6]. For instance, Gibert et al. [1] have utilized the lumped parameter approach. Chae et al. [2], Biermann and Hagerodt [4], and Menday et al. [6] have implemented the multi-body dynamics or the finite element methods. Biermann and Hagerodt [4] have also tried to simulate possible real-life clunk conditions in their experimental set-ups. Nevertheless, the current industrial practice and the scientific investigations show that clunk and the like phenomena are not clearly understood and no specific simulation tools and analytical models are available since many different vehicle elements and clearance non-linearities are encountered.

In order to properly address this problem, a suitable non-linear simulation model is needed since backlashes between the gear pairs or splines, as well as other clearances within the driveline system could potentially induce impacts between the moving parts and thus generate clunk-type noise and vibration problems [1-7]. In particular, Couderc et al. [8] analyzed the torsional vibration of a driveline when subjected to a torque pulse; their models included two non-linear elements, such as a multi-valued clutch damper and a gear pair with backlash. Further, Singh et al. [9-11] have developed comprehensive models of gear rattle and they have examined the non-linear behavior of multi-staged clutch dampers and gear pairs with backlashes, under unloaded and loaded conditions. The chief goal of this research is therefore to develop a suitable non-linear model that would describe the essential characteristics of clunk and to conduct key parametric design studies for reduced noise and vibration. A new mathematical simulation model for a front wheel drive system is developed and typical clunk transient results under simplified but alternate tip-in and tip-out conditions are presented. Furthermore, four new metrics are proposed to define or quantify the severity of clunk. On a more fundamental note, we assess the interactions among the non-linearities within the context of impulsive responses.

## PROBLEM FORMULATION

Consider a driveline transient problem (clunk) under a tip-in or tip-out driving condition that occurs in a 4x2 front-wheel drive (FWD) medium passenger vehicle, equipped with a dual-axis type 5-speed manual transmission as shown in Figure 1. We focus on the source of the problem and not on the path and receiver issues. Accordingly we consider multi-degree of freedom lumped parameter torsional system such as the one shown in Figure 2; the transmission is assumed to be in the 3rd engaged gear. We examine only the torsional parameters of each driveline component or sub-system, such as inertias (I), stiffness (K), and damping (C). No coupling effect between torsion and driveline system

flexure is considered. It is assumed that the parameters of the models shown in Figures 2 and 3 could be obtained by analytical or experimental methods [12]. To construct the viscous damping matrix, a damping ratio of 5% is used for all modes of interest. A large dimensional system (Figure 2) is first created, and then a model reduction process is carried out to develop the 7-DOF system of Figure 3. The validity of the model reduction is demonstrated by comparing the undamped eigensolutions of the linearized models. The non-linear model of Figure 3 includes the following non-linear components: a multi-staged clutch damper (with hysteresis), 2 gear pairs with backlashes and 2 in spline interfaces with backlashes. All such elements are introduced to conceptually address the clunk issues and to better understand dynamic interactions between various non-linear sources. Again, the transmission is assumed to be in the 3rd engaged gear, and the clutch is mathematically activated to sharply change the mean torque values, which are based on a mean engine torque-speed-throttle angle map [10]. The torque rise or drop time histories and shapes are assumed and comparatively evaluated. Further, the drag torque within the transaxle is estimated as a non-linear function of the engine speed and operating temperature [10]. The road resistance is also considered as a function of the vehicle speed [12]. Thus, the overall drag terms would vary with time as well. The non-linear model is numerically solved in time domain using a stiff differential equations solver that was developed earlier for gear rattle problems [11]. The impulsive behavior under two different vehicle conditions, namely the throttle tip-in and tip-out, is predicted.

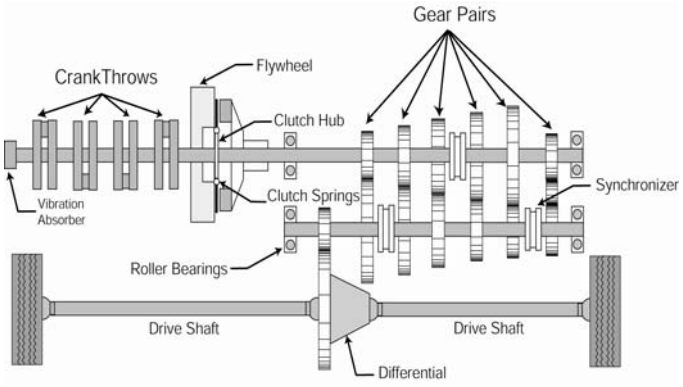


Figure 1 Example case: 4x2 front wheel drive system with manual transmission.

Specific objectives of this paper are as follows. First, develop a lumped parameter torsional model including multiple clearance-type non-linear characteristics which are capable of inducing transient clunk events. Second, investigate the nature of throttle tip-in and tip-out clunk phenomena by predicting the time domain signatures of absolute and relative angular displacement, velocities, accelerations, and elastic torques. Third, observe the conditions for single or double-sided impacts and correlate them with excitation events and/or transitions within the clearance non-linearities. Fourth, propose new clunk metrics and use them to examine typical simulation results. Finally, examine the role of critical design parameters. The space constraints for this paper will limit us from a detailed discussion of all studies, and thus only the conceptual formulations and illustrative results will be presented.

## LINEAR MODELS

Figure 2 schematically shows the lumped parameter torsional model of a 4x2 front-wheel drive automotive system with a manual transmission. It has been shown that the lumped parameter approach is sufficiently accurate to investigate clunk or similar transient phenomena in the driveline system [1, 3]. In order to develop a suitable non-linear model, the original system with 19-DOF in Figure 2 is replaced by a reduced order model with 7-DOF that is shown in Figure 3, while retaining all of the significant dynamic characteristics. Since clunk is mostly initiated in loaded gear pairs [5], the inertias for all unloaded transmission gears ( $I_{GO1}$ , $I_{GO2}$ , $I_{GI4}$ , $I_{GO5}$ , $I_{GI}$ , and $I_{GOR}$ ) for the third engaged gear case is lumped into either input shaft ( $I_{IS}$ ) or output shaft ( $I_{OS}$ ) inertias by using the inertia reduction method [10]. An insight into the model development process can be gained by examining natural frequencies and modes of the linearized driveline system over the frequency range of interest.

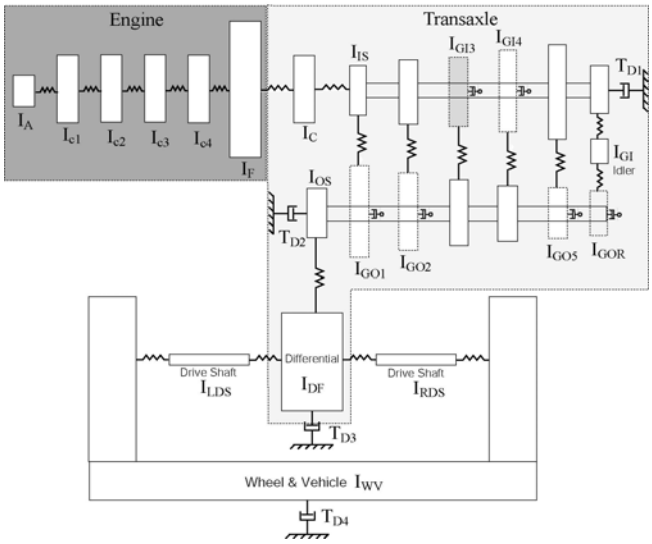


Figure 2 Linear torsional model of the example case: 19-DOF undamped system in the 3rd engaged gear.

Now, consider the equations of motion for the 7-DOF (or 19-DOF) linear, undamped and unforced system in matrix form, where $\underline{\underline{M}}$ is the inertia matrix, $\underline{\underline{K}}$ is the stiffness matrix, and $\underline{\theta}$ is the generalized torsional displacement vector.

$$\underline{\underline{M}}\,\underline{\ddot{\theta}}(t) + \underline{\underline{K}}\,\underline{\theta}(t) = \underline{0} \qquad (1)$$

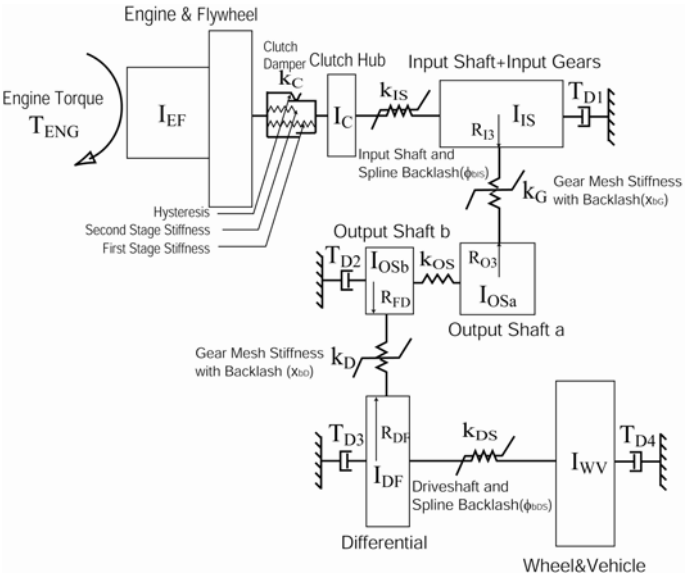


Figure 3 Non-linear torsional model of the example case in the 3rd engaged gear: 7-DOF system with a multi-staged clutch damper and multiple gear pairs and hub-spline interfaces with backlashes.

The 7-DOF system of Figure 3 is linearized by assuming that all gear pairs remain in contact (with linear mesh stiffness) and only the second stage of clutch damper (with linear stiffness $k_C$ ) is operational with zero hysteresis. Accordingly, torsional system matrices of the 7-DOF model are expressed as follows; similar expressions can be defined for the 19-DOF of Figure 2.

$$\underline{\underline{M}} = diag(I_{EF}, I_C, I_{IS}, I_{OSa}, I_{OSb}, I_{DF}, I_{WV}) \tag{2}$$

$$\underline{\underline{K}} = \begin{bmatrix} k_C & -k_C & 0 & 0 & 0 & 0 & 0 \\ -k_C & k_C + k_{IS} & -k_{IS} & 0 & 0 & 0 & 0 \\ 0 & -k_{IS} & k_{IS} + R^2_{I3} k_G & R_{I3} R_{O3} k_G & 0 & 0 & 0 \\ 0 & 0 & R_{I3} R_{O3} k_G & R^2_{O3} k_G + k_{OS} & -k_{OS} & 0 & 0 \\ 0 & 0 & 0 & -k_{OS} & R^2_{FD} k_D + k_{OS} & R_{FD} R_{DF} k_D & 0 \\ 0 & 0 & 0 & 0 & R_{FD} R_{DF} k_D & R^2_{DF} k_D + k_{DS} & -k_{DS} \\ 0 & 0 & 0 & 0 & 0 & -k_{DS} & k_{DS} \end{bmatrix} \tag{3}$$

The subscripts for the torsional inertia (I) and stiffness (k) elements are denoted in Figure 3. Relevant gear radii are defined by the input gear $R_{I3}$ , output gear on the counter shaft $R_{O3}$ , final driving gear $R_{FD}$ , and the differential driving gear $R_{DF}$ . Both 7 and 19 degree of freedom models are simulated to yield undamped eigensolutions to examine the validity of model the reduction process. Table 1 compares torsional natural frequencies and mode shapes. Each eigenvector is normalized with respect to the largest torsional displacement, which is then set to 1.0. At the surging mode at 7.5 Hz in the 19-DOF model, the engine and flywheel witness the largest displacement 0.998 instead of 1.0 since the crankshaft between the last crank throw and flywheel experiences a minor torsional deformation. Since all torsional mode shapes and natural frequencies match well, the reduced order 7-DOF model is deemed to possess all of essential dynamic characteristics of the original 19-DOF model up to at least 350 Hz.

Next, the damping matrix $\underline{\underline{C}}$ is constructed with modal damping ratios $\zeta_r$ . For this research, $\zeta_r = 0.05$ , (or 5%) is used for all modes.

Finally, the torque excitation vector is expressed as follows where $T_{ENG}(t)$ is engine torque, $T_{D1}(t)$ is drag torque on input shaft, $T_{D2}(t)$ is drag torque on the output shaft, $T_{D3}(t)$ is drag toque on differential, and $T_{D4}(t)$ is total road resistance.

$$\underline{T}(t)^T = \left[T_{ENG}(t), 0, -T_{D1}(t), 0, T_{D2}(t), -T_{D3}(t), -T_{D4}(t)\right] \tag{4}$$

The equations are assembled for either 7-DOF or 19-DOF system as:

$$\underline{\underline{M}}\,\underline{\ddot{\theta}} + \underline{\underline{C}}\,\underline{\dot{\theta}} + \underline{\underline{K}}\,\underline{\theta} = \underline{T}(t) \tag{5}$$

This model could be used to analytically or numerically determine the transient and steady state responses given a specific input as defined by (4). The clunk problem is introduced by component non-linearities, which are illustrated in the next section.

## NON-LINEAR MODEL

### EXCITATION AND DRAG TORQUES

The excitation torque $T_{ENG}(t)$ can be typically decomposed into a time-varying mean $T_m(t)$ and pulsating $T_p(t)$ torque term and expressed via the Fourier series expansion as

$$T_{ENG}(t) = T_m(t) + \sum_{n=1}^{\infty} T_{pn} \sin(n\Omega_p t + \varphi_n) \tag{6}$$

Only the mean $T_m(t)$ term is used here since this study focuses on the transient responses. Note, the engine torque oscillations will not change the nature of the solutions with respect to clunk. $T_m(\Omega_{ENG}, \Phi_{th})$ is estimated by utilizing a mean engine torque-speed $\Omega_{ENG}$ - throttle angle $\Phi_{th}$ map [10]. In the simulation, throttle is assumed to tip-in from zero $\Phi_{th}$ to a positive $\Phi_{th}$ , or tip-out from positive $\Phi_{th}$ to zero $\Phi_{th}$ with the throttle up or down over specified rise or fall times. In the tip-in study, $T_m$ is varied from -20 (closed throttle at about 2500 rpm) to 80 N-m (40 deg. throttle angle at about 2500 rpm). Likewise, $T_m$ is varied from 80 to -20 N-m for the tip-out study. In both cases, three time histories are assumed. Then the transaxle drag torques $T_{D1-D3}(\Omega_{ENG}, \Gamma)$ are calculated. They are directly related to the gear box oil viscosity which is a function of oil temperature $\Gamma$ and the mean

engine speed $\Omega_{ENG}$ according to the following expressions where $T_{Do}$ is the reference drag [10].

$$T_{Di}(\Omega_{ENG},\Gamma) = T_{Do} g_{\Gamma}(\Gamma) g_{\Omega}(\Omega_{ENG}), \quad i = 1,2,3 \tag{7a}$$

$$g_{\Gamma}(\Gamma) = e^{-d\Gamma}, \; g_{\Omega}(\Omega_{ENG}) = a_1 + a_2(\Omega_{ENG}) + a_3(\Omega_{ENG})^2 \tag{7b,c}$$

$$T_{RT}(\Omega_{ENG},\Gamma) = T_{D1}(\Omega_{ENG},\Gamma) + \alpha_G T_{D2}(\Omega_{ENG},\Gamma) + \alpha_G \alpha_D T_{D3}(\Omega_{ENG},\Gamma) \tag{7d}$$

Both functions $g_{\Gamma}(\Gamma)$ and $g_{\Omega}(\Omega_{ENG})$ and their coefficients $a_1$, $a_2$, $a_3$, and $d$ are determined using specific transaxle data and reference [10]. To obtain the torque resistance $T_{RT}(\Omega_{ENG},\Gamma)$, which will be shown later, two speed ratios $\alpha_G = (R_{I3}/R_{O3})$ and $\alpha_D = (R_{I3}/R_{O3})(R_{FD}/R_{DF})$ are applied in equation (7d)

The total road drag $T_{D4}(t)$ (applied to the wheel and vehicle body) includes contributions from road contact rolling, aerodynamics, and road grade [12]. Further, the effect of brake resistance $T_{brake}(t)$ could also be added. To obtain the total torque resistance $T_{RR}(t)$, multiply $T_{D4}(t)$ further by the drivetrain speed ratio $\alpha_G \alpha_D$.

$$T_{D4}(t) = T_a(t) + T_g(t) + T_r(t) + T_{brake}(t) \tag{8a}$$

$$T_{RR}(t) = \alpha_G \alpha_D \left(T_a(t) + T_g(t) + T_r(t) + T_{brake}(t)\right) \tag{8b}$$

The governing equations for the non-linear system of Figure 3 are described below where $T_C$, $T_{IS}$, $T_{DS}$, $F_G$, and $F_D$ describe the interfacial torques or forces due to the clearance non-linearities. Further, the external torques include the drag torque terms ($T_{D1}(t)$ on the input shaft, $T_{D2}(t)$ on the output shaft, $T_{D3}(t)$ on differential, and $T_{D4}(t)$ on the total road resistance) and the engine torque $T_{ENG}(t)$,

$$I_{EF}\ddot{\theta}_{EF} + T_C(\theta_{EF+C},\dot{\theta}_{EF+C}) + C_C(\dot{\theta}_{EF+C}) = T_{ENG}(t)$$

$$I_C\ddot{\theta}_C - T_C(\theta_{EF+C},\dot{\theta}_{EF+C}) + T_{IS}(\phi_{rIS},\phi_{bIS}) - C_C(\dot{\theta}_{EF+C}) + C_{IS}(\dot{\theta}_{C+IS}) = 0$$

$$I_{IS}\ddot{\theta}_{IS} - T_{IS}(\phi_{rIS},\phi_{bIS}) + R_{I3}F_G(x_{rIS},x_{bIS}) - C_{IS}(\dot{\theta}_{C+IS}) + C_G(\dot{\theta}_{IS+OSa}) = -T_{D1}(t)$$

$$I_{OSa}\ddot{\theta}_{OSa} + K_{OS}(\theta_{OSa} - \theta_{OSb}) + R_{O3}F_G(x_{rG},x_{bG}) - C_G(\dot{\theta}_{IS+OSa}) + C_{OS}(\dot{\theta}_{OSa+OSb}) = 0$$

$$I_{OSb}\ddot{\theta}_{OSb} - K_{OS}(\theta_{OSa} - \theta_{OSb}) + R_{FD}F_D(x_{rD},x_{bD}) - C_{OS}(\dot{\theta}_{OSa+OSb}) + C_D(\dot{\theta}_{OSb+DF}) = T_{D2}(t)$$

$$I_{DF}\ddot{\theta}_{DF} + T_{DS}(\phi_{rDS},\phi_{bDS}) + R_{DF}F_D(x_{rD},x_{bD}) - C_D(\dot{\theta}_{OSb+DF}) + C_{DS}(\dot{\theta}_{DF+DS}) = -T_{D3}(t)$$

$$I_{WV}\ddot{\theta}_{WV} - T_{DS}(\phi_{rDS},\phi_{bDS}) - C_{DS}(\dot{\theta}_{DF+DS}) = -T_{D4}(t) \tag{9-15}$$

CLUTCH DAMPER MODEL

Consider the non-linear characteristics of an asymmetric dual-staged clutch damper of Figure 4. The non-linear clutch torque $T_C$ is expressed as a function of the relative displacement $\theta_{EF+C} = \theta_{EF} - \theta_C$ and the relative velocity $\dot{\theta}_{EF+C} = \dot{\theta}_{EF} - \dot{\theta}_C$, and is defined by the sum of elastic $T_S$ and hysterestic $T_H$ torque terms.

$$T_C(\theta_{EF+C},\dot{\theta}_{EF+C}) = T_S(\theta_{EF+C}) + T_H(\theta_{EF+C},\dot{\theta}_{EF+C}) \tag{16}$$

The elastic torque $T_S(\theta_{EF+C})$ is controlled by torsional stiffnesses ($k_{C11}$, $k_{C21}$, $k_{C12}$, and $k_{C22}$) and transition angles ($\phi_{11}$ and $\phi_{12}$) as shown in Figure 4.

$$T_S(\theta_{EF+C}) = \begin{cases} k_{C21}\phi_{11} + k_{C2}(\theta_{F+C} - \phi_{11}), & \theta_{EF+C} > \phi_{11} \\ k_{C11}\phi_{11}, & 0 < \theta_{EF+C} < \phi_{11} \\ k_{C12}\phi_{12}, & \phi_{12} < \theta_{EF+C} < 0 \\ -k_{C22}\phi_{12} + k_{C12}(\theta_{F+C} - \phi_{12}), & \theta_{EF+C} < \phi_{12} \end{cases} \tag{17a-d}$$

Similarly, the hysterestic torque $T_H$ is modeled as a function of $\theta_{EF+C}$ and $\dot{\theta}_{EF+C}$. It is formulated below in terms of $H_1$ and $H_2$ which represent the hysteresis values of the first and second stages, respectively,

$$T_H(\theta_{EF+C},\dot{\theta}_{EF+C}) = \frac{1}{2}\begin{cases} H_2 + (H_2 - H_1)\,sign(\theta_{EF+C} + \phi_{12}), & \dot{\theta}_{EF+C} > 0 \\ -H_2 + (H_2 - H_1)\,sign(\theta_{EF+C} + \phi_{11}), & \dot{\theta}_{EF+C} < 0 \end{cases} \tag{18a,b}$$

Here, the sign function with argument x is given below and graphically shown in Figure 5.

$$sign(\mathrm{x}) = \begin{cases} 1, & \mathrm{x} > 0 \\ 0, & \mathrm{x} = 0 \\ -1, & \mathrm{x} < 0 \end{cases} \tag{19}$$

Since the $sign(\mathrm{x})$ is a discontinuous non-analytical function, the continuous analytical function $\xi(x,\sigma)$ [9-11] is used to smoothen it, and the conditioning factor $\sigma$ controls the smoothness of the curve as seen in Figure 5.

$$sign(\mathrm{x}) \approx \xi(\mathrm{x},\sigma) = \frac{2}{\pi}\arctan(\sigma \mathrm{x}) \tag{20}$$

A sufficiently large value of $\sigma$ is recommended for non-linear analyses, particularly to observe vibro-impacts [11]. In the models, all discontinuities are approximated with equation (20), and an appropriate value of $\sigma$ (such as $> 10^5$) is used based on experience.

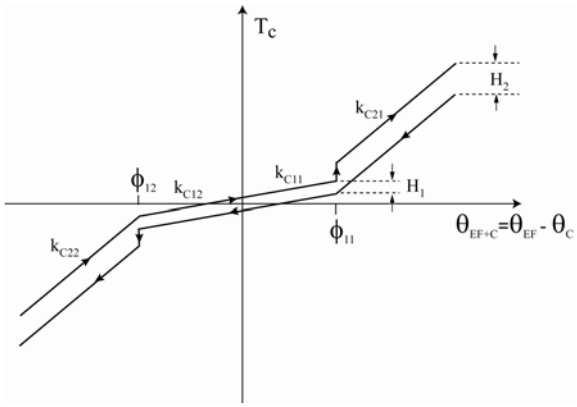


Figure 4 Non-linear characteristics of a dual-staged clutch damper.

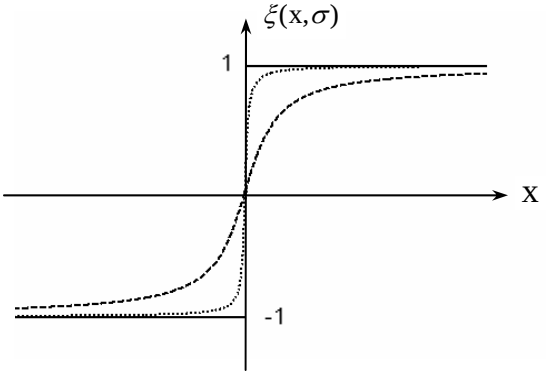


Figure 5 Effect of smoothening on the sign function. Key: — discontinuous $sign(x)$, ----- $\xi(x,\sigma)$ with $\sigma=10$, ..... $\xi(x,\sigma)$ with $\sigma=100$.

$$T_S(\theta_{EF+C}) = k_{C11}\theta_{EF+C} + T_{SP1} - T_{SP2} + T_{SN1} - T_{SN2}$$

$$T_{SP1} \approx 0.5k_{C21}\left[2\theta_{F+C} + \left((\theta_{EF+C}-\phi_{11})\xi(\theta_{EF+C}-\phi_{11},\sigma) - (\theta_{EF+C}+\phi_{11})\right)\right]$$

$$T_{SP2} \approx 0.5k_{C11}\left[2\theta_{F+C} + \left((\theta_{EF+C}-\phi_{11})\xi(\theta_{EF+C}-\phi_{11},\sigma) - (\theta_{EF+C}+\phi_{11})\right)\right]$$

$$T_{SN1} \approx 0.5k_{C22}\left[2(-\phi_{12}) + \left((\theta_{EF+C}+\phi_{12}) - (\theta_{EF+C}-\phi_{12})\xi(\theta_{EF+C}-\phi_{12},\sigma)\right)\right]$$

$$T_{SN2} \approx 0.5k_{C12}\left[2(-\phi_{12}) + \left((\theta_{EF+C}+\phi_{12}) - (\theta_{EF+C}-\phi_{12})\xi(\theta_{EF+C}-\phi_{12},\sigma)\right)\right]$$

(21a-d)

Here, $k_{Ci1}$ represents the $i^{th}$ stage stiffness on the positive side, $k_{Ci2}$ represents the $i^{th}$ stage stiffness on the negative side, $T_{SP1}$ (or $T_{SP2}$) represents the positive side torque, and $T_{NP1}$ (or $T_{NP2}$) represents the negative side torque. Next, replace the sign function by $\xi(x,\sigma)$ in equations (18a) and (18b) to yield the following equations,

$$T_H(\theta_{EF+C},\dot{\theta}_{EF+C}) \approx 0.5\left[H_2 + \left(H_2 - H_1\right)\xi(\theta_{EF+C}+\phi_{12},\sigma)\right],\ \dot{\theta}_{EF+C} > 0$$

$$T_H(\theta_{EF+C},\dot{\theta}_{EF+C}) \approx 0.5\left[-H_2 + \left(H_2 - H_1\right)\xi(\theta_{EF+C}+\phi_{11},\sigma)\right],\ \dot{\theta}_{EF+C} < 0$$

(22a-b)

Combine equations (22a) and (22b) to yield one governing equation,

$$T_H(\theta_{EF+C},\dot{\theta}_{EF+C}) \approx 0.5\xi(\dot{\theta}_{EF+C},\sigma)H_2 + 0.25\left(H_2 - H_1\right)$$
$$\times\left[\xi(\theta_{EF+C}+\phi_{11},\sigma)(1-\xi(\dot{\theta}_{EF+C},\sigma)) + \xi(\theta_{EF+C}+\phi_{12},\sigma)(1-\xi(\dot{\theta}_{EF+C},\sigma))\right]$$

(23)

SPLINE AND GEAR PAIR MODELS

The non-linear gear mesh forces $F_G$ and $F_D$ (N) and hub-spline interface torques $T_{IS}$ and $T_{DS}$ (N-m) include a linear contact stiffness element and backlash. Each is modeled using the following non-linear, non-dimensional function $\bar{f}(\delta,b)$ that is shown in Figure 6 (a). Here, $\delta$ is the relative (non-dimensional) displacement, the contact stiffness is unity ($|\delta| > |b|$) and the backlash regime is from $\delta = b$ to $\delta = -b$. Again, non-analytical function $\bar{f}(\delta,b)$, which is defined in equation (24a), is approximated using the smoothening function in equation (24b).

$$\bar{f}(\delta,b) = \begin{cases} \delta - b, & \delta > b \\ 0, & -b \le \delta \le b \\ \delta + b, & \delta < b \end{cases} \quad (24a)$$

$$\bar{f}(\delta,b) \approx \delta + 0.5(\delta - b)\xi(\delta - b,\sigma) - (\delta + b)\xi(\delta + b,\sigma) \quad (24b)$$

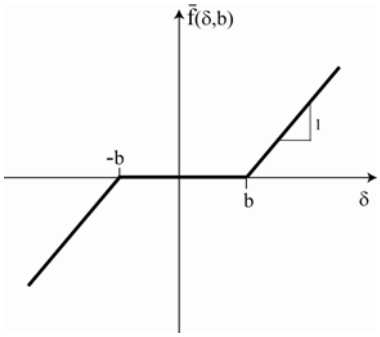


(a)

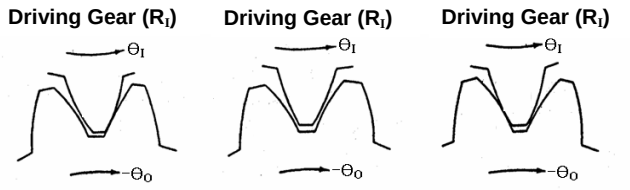


(b) (c) (d)

Figure 6 Inclusion of backlash in gear mesh forces or spline interface torques. (a) Non-dimensional non-linear function (b) gears are in contact on the driving side $(x_r > x_b)$ (c) gears are separated in the backlash regime $(-x_b < x_r < x_b)$ and (d) gears are in contact on the driven side $(x_r > x_b)$. Here $x_r = R_I\theta_I + R_O\theta_O$ and $x_b$ corresponds to $b$ in (a).

With reference to Figure 3, the gear mesh forces $F_G$ and $F_D$ are written as follows where the dynamic force between mating teeth acts along the line of action, $x_{rG}$ and $x_{rD}$ are the relative linear displacements at the contact points, $x_{bG}$ and $x_{bD}$ are the gear backlashes, and $k_G$ and $k_D$ are linearized mesh stiffnesses. In the cases of Figure 6 (b) and (d), the non-zero forces are characterized by the linear gear mesh stiffness. And, when the gears are separated, the mesh force is zero, such is the case in Figure 6 (c).

$$F_G(x_{rG}, x_{bG}) = k_G \cdot \bar{f}(x_{rG}, x_{bG}) \tag{25}$$

$$F_D(x_{rD}, x_{bD}) = k_D \cdot \bar{f}(x_{rD}, x_{bD}) \tag{26}$$

Likewise, the hub-spline interface torques $T_{IS}$ and $T_{DS}$ of Figure 3 are given as follows where $\phi_{rIS}$ and $\phi_{rDS}$ are the relative angular displacements, $\phi_{bIS}$ and $\phi_{bDS}$ are the hub-spline backlashes, and $k_{IS}$ and $k_{DS}$ are the hub-spline stiffnesses.

$$T_{IS}(\phi_{rIS}, \phi_{bIS}) = k_{IS} \cdot \bar{f}(\phi_{rIS}, \phi_{bIS}), \tag{27}$$

$$T_{DS}(\phi_{rDS}, \phi_{bDS}) = k_{DS} \cdot \bar{f}(\phi_{rDS}, \phi_{bDS}) \tag{28}$$

NUMERICAL SOLUTION

Finally, given the governing equations, the torque excitation $T_m(t)$ and the drag terms, the initial displacements and velocities of each inertial element can be determined. Further, equations are non-dimensionalized and examined as suggested in references [10, 11]. The non-linear model is then solved using a 4/5$^{th}$ order Runge-Kutta integration routine with a variable integration time step [9].

## ILLUSTRATIVE RESULTS

Figures 7 and 8 show typical clunk responses during tip-in and tip-out events, respectively. During the tip-in example of Figure 7, it is evident that all gears and splines on the driven side start to lose contact at point A, travel independently through the backlashes from A to B, and land on the driving side at B. The first closing impacts are observed at B and result in impulsive accelerations and interfacial torques. Additional backlash opening and closing events at C and D result in double-sided impacts. Similarly, during the tip-out example of Figure 8, all gears on the driving side start to separate at A and then each pair makes successive contacts on the driven side at B and C. Similar clunk events are observed at D, E, and F. This is because the torsional oscillations subsequent to the first impact force the inertial elements to travel through the backlash regimes, again, causing additional impacts.

## METRICS TO EVALUATE THE SEVERITY OF CLUNK

In the case of clunk, one must obviously quantify the instantaneous peaks of impulsive events while also considering the number and nature of the impacts. Accordingly, typical impulsive responses are investigated during the clunk events. As the inertial elements within the driveline oscillate due to the first hard closing impact, the gears may separate and travel across each lash regime leading to additional impacts. Depending on the drag torques and other loads, such impacts may take place on one side of the gears (with one or more single-sided impacts), or in a severe case, gear teeth may impact on both driving and driven sides, resulting in one or more double-sided impacts. Such types of impacts are easily observed from the relative displacement responses across lash regimes. Metrics could be developed based on the peak to peak impulsive motions (in torsional or translational velocity or acceleration units) that occur across the gears or splines; these could be correlated to the vehicle sound and vibration signatures that would be generated assuming the knowledge of paths and receivers. Yet, another indicator of the clunk severity could be the magnitude of a change in the energy or momentum associated with the clunk event. In practice, the radiated sound pressure may be controlled by a particular component with the highest impact energy. For instance, consider two rigid interacting bodies or gears (such as 1 and 2) that suddenly come in contact. At the instant an impact occurs, both experience a gain or loss ($\Delta$) in kinetic energies $(KE)$ that are assumed to equal in magnitude, opposite in direction, such that $\Delta KE1 = -\Delta KE2$ . We assume that the impact energy is proportional to the $|\Delta KE1 - \Delta KE2|$ at each lash location. Using this argument, we are able to conclude that the final drive gear pair transfer the highest impact energy to the driveline and then to the vehicle body. Selected experiments have shown that the dominant source of clunk is the gear pair in the final drive, particularly for the higher frequency clunk [2, 4]. Based on the above mentioned criteria, 4 metrics are proposed in Table 2 that would attempt to quantify the clunk. First, a change in the instantaneous torsional velocity (or speed in RPM) during impact could be used to evaluate a change in the momentum at the instant an impulse occurs. Second, the gear mesh or spline interfacial contact torques that are generated at the point of impact can be calculated. Third, instantaneous accelerations that are generated due to impulsive contact forces or torques are examined to assess the effects on the structural dynamics at higher frequencies. Fourth, the type of impacts is quantified in terms of single or double sided impacts as this knowledge may correlate well with human (subjective) response.

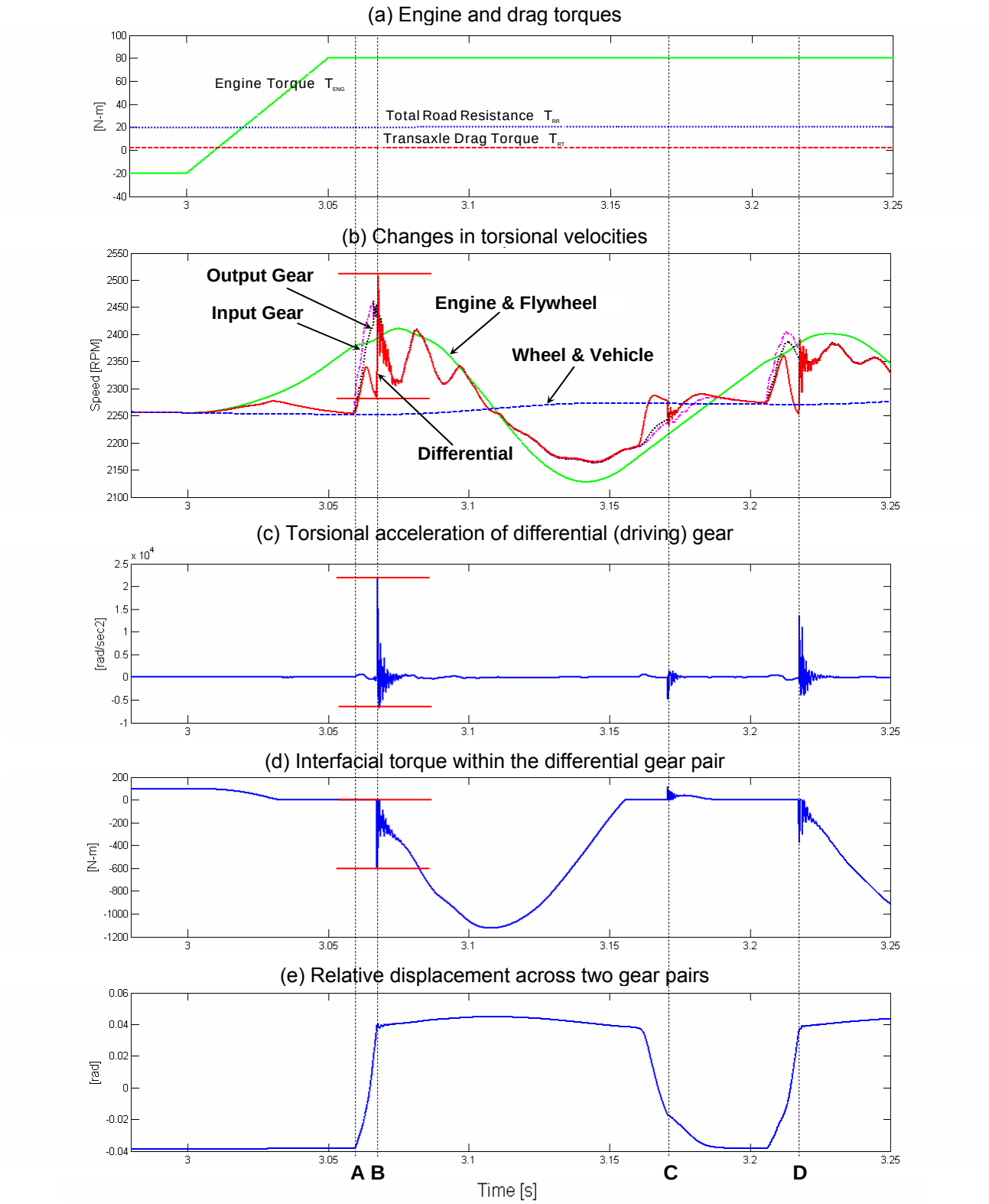


Figure 7 Clunk events in the non-linear model of Figure 3 with a dual clutch damper during the tip-in event (a) Assumed engine torque B as defined in Figure 9 and drag terms; (b) $\dot{\theta}_{EF}$ , $\dot{\theta}_{IS}$ , $\alpha_G\dot{\theta}_{OSa}$ , $\alpha_G\alpha_D\dot{\theta}_{DF}$ , $\alpha_G\alpha_D\dot{\theta}_{WV}$ ; (c) $\ddot{\theta}_{DF}$ ; (d) $R_{DF}F_D$ ; (e) $\theta_{IS}-\alpha_G\alpha_D\theta_{DF}$ . Here **A,B,C** and **D** represent events of interest.

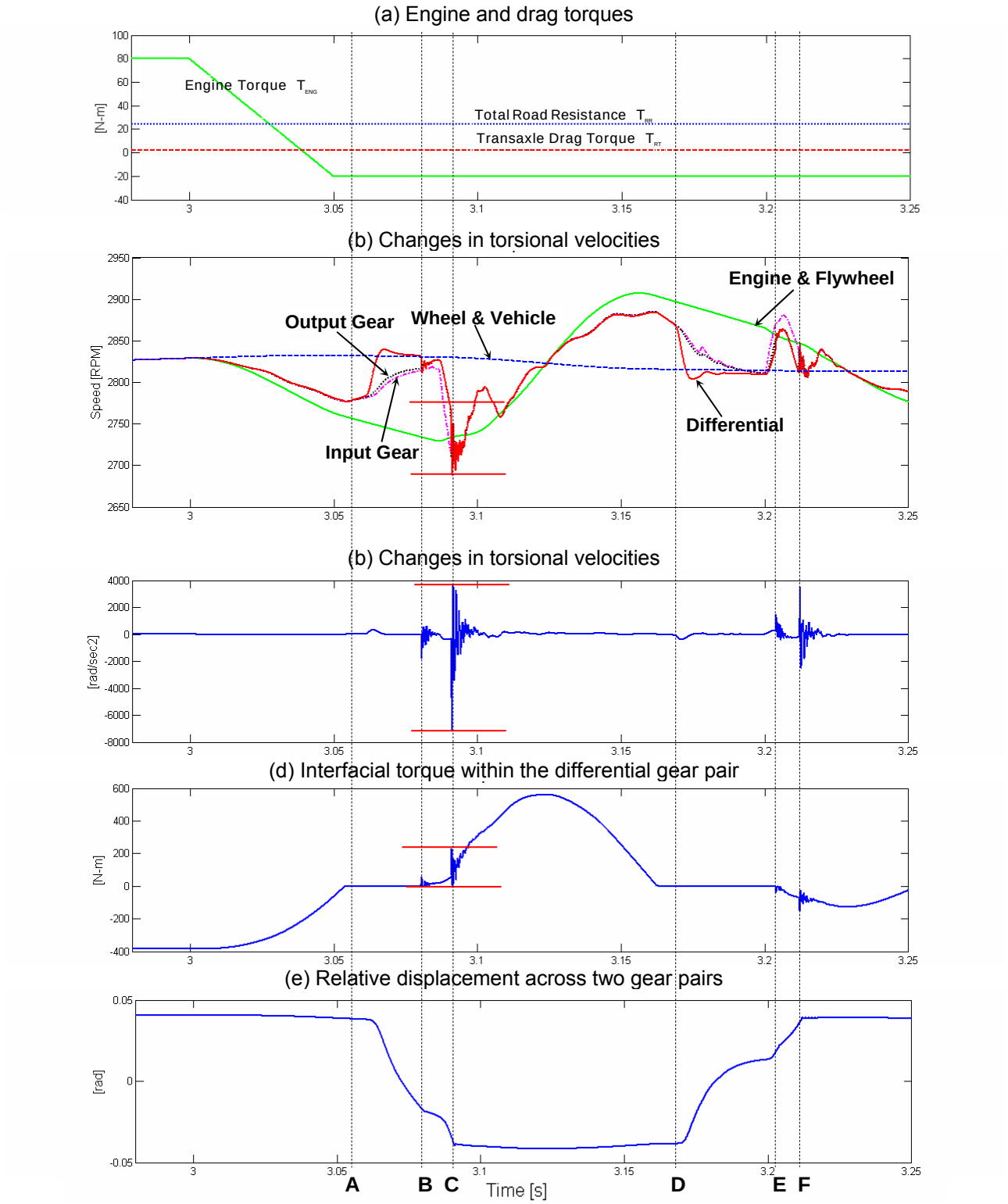


Figure 8 Clunk events in the non-linear model of Figure 3 with a dual clutch damper during the tip-out event (a) Assumed engine torque B as defined in Figure 9 and drag terms; (b) $\dot{\theta}_{EF}$ , $\dot{\theta}_{IS}$ , $\alpha_G\dot{\theta}_{OSa}$ , $\alpha_G\alpha_D\dot{\theta}_{DF}$ , $\alpha_G\alpha_D\dot{\theta}_{WV}$ ; (c) $\ddot{\theta}_{DF}$ ; (d) $R_{DF}F_D$ ; (e) $\theta_{IS}-\alpha_G\alpha_D\theta_{DF}$ . Here **A,B,C** and **D** represent events of interest.

## PARAMETERIC DESIGN STUDIES

### EFFECT OF TIP-IN OR TIP-OUT TIME HISTORIES

It has been shown that the engine torque rise or fall rate has a distinct effect on the severity of clunk [2, 3]. Three simplified torque shapes during each event, with assumed rise or fall rates as shown in Figure 9, are conceptually evaluated to assess this claim. Torque A is a typical step function with zero rise time, torque B ascends linearly with a rise time of 50 ms, and torque C grows exponentially with a time constant of 50 ms. According to the results of Tables 3 and 4, one may conclude that a smoother rise or fall in $T_{ENG}(t)$ (such as torque C) would be more desirable since it leads to a smooth engagement at the backlash and reduced impulses within the driveline. The torque transferred from the engine to driveline should be as low as possible until after all lashes are passed through. However, it is not practical to use a very low value of torque as it may adversely affect the costumer's perception of vehicle acceleration.

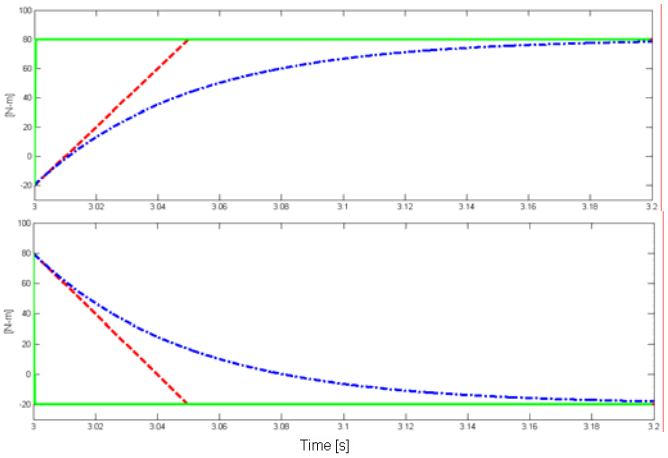


Figure 9 Simplified engine torque shapes $T_{ENG}(t)$ for tip-in and tip-out events. Key: Torque A Torque B Torque C.

### EFFECT OF CLUTCH DAMPER PARAMETERS

The effect of dual-staged clutch damper tuning is examined next as it may affect the torque that is transferred between the engine and the driveline. During tip-out, the motion within the clutch is initiated in second stage on the positive side of stiffness $k_{C21}$, and then a rapid transfer is observed to the negative side of the clutch stiffness $k_{C22}$ via the pre-damper stiffnesses $k_{C12}$ and $k_{C11}$. According to Table 5, the $Q_1$, $Q_2$ and $Q_3$ values are much more sensitive to a change in $k_{C11}$ (= $k_{C12}$) than $k_{C21}$ (= $k_{C22}$). Tuning of $k_{C21}$ (= $k_{C22}$) alone is not desirable to reduce clunk since torque capacities would be affected. Thus, low rate stiffnesses must be properly selected for reducing clunk.

### EFFECT OF NUMBER OF BACKLASHES

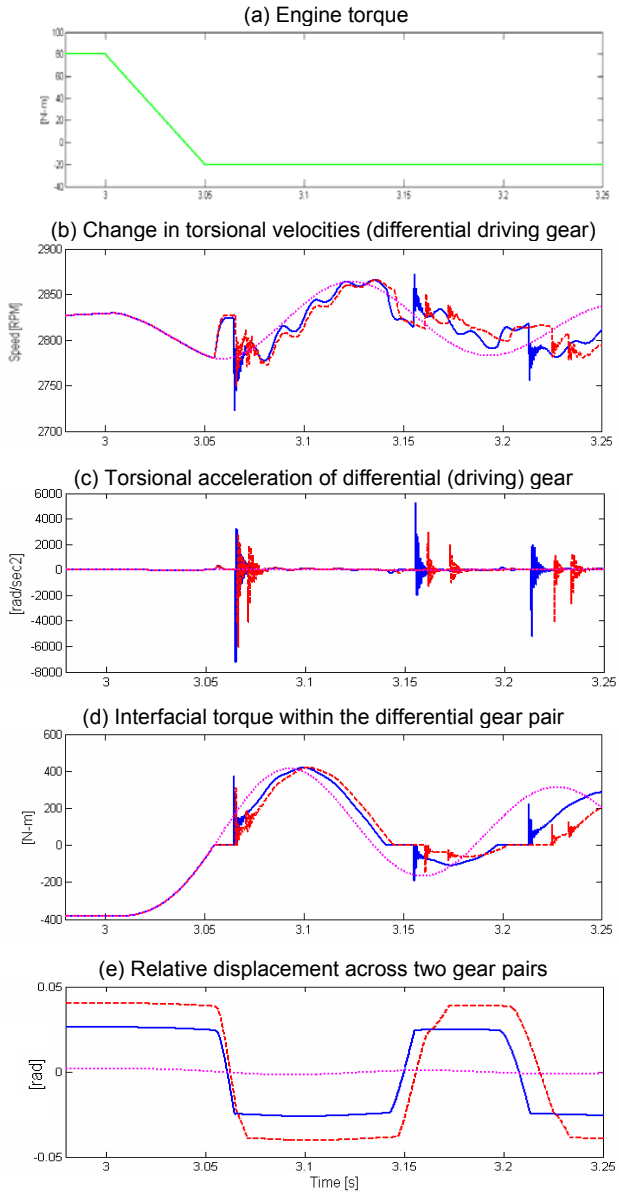


Figure 10 Comparison of impulsive behavior between zero, one, and two backlash elements during the tip-out event. Key: One Backlash Two Backlashes Zero Backlash (a) Assumed engine torque B as defined in Figure 9; (b) $\alpha_G \alpha_D \dot{\theta}_{DF}$; (c) $\ddot{\theta}_{DF}$; (d) $R_{DF} F_D$; (e) $\theta_{IS} - \alpha_G \alpha_D \theta_{DF}$.

Figure 10 shows the effect of the number of backlashes on clunk. The non-linear model with one backlash (in the differential gear pair) is compared to the one with two backlashes (in the input and the differential gear pairs), and for the sake of comparison, the case of zero backlash is also presented; this can be simulated with either the non-linear model or with analytical solutions that arise from the linear model given by equation (5). As seen in Figure 10, when two backlashes are used, two consecutive impacts occur within the differential gear pair, instead of only one impact that is observed when a single backlash element is used. However, each

impulsive event with a single backlash is higher in amplitude when compared to the corresponding amplitude with two gear backlashes. Clearly, the oscillation is sinusoidal without any lash, as the first mode is excited. Thus, the clunk severity is not necessarily related to the cumulative backlash, though the general practice is to simply calculate the cumulative backlash as a rough measure of clunk. However, considerable change in the cumulative backlash value may be needed to produce a significant change in the clunk response.

## CONCLUSION

A non-linear model has been developed specifically to examine the clunk problem, and it effectively shows dynamic interactions among various components. In particular, the results reveal sudden motions of inertial components across the lash regimes, and consequently, single and double-sided impacts occur. Based on these results, the clunk severity can be objectively assessed. Four metrics have been proposed, based on the impulsive torsional responses within the final drive gear pair, which seems to produce the highest energy at impact. Further, the sensitivity studies using these metrics suggest the following conclusions or design solutions: 1. Keep the instantaneous torque that is transferred from the engine to the driveline as low as possible until all lashes are passed through; 2. The clunk severity is more sensitive to a change in the stiffness of the pre-damper stage (first stage) than that of the driving-side stage (second stage); 3. The clunk severity may not increase linearly with the cumulative backlash value. Future work will investigate clunk problems in RWD or AWD systems with an automatic transmission [13]. Finally, more computational work needs to be carried out to better understand the nature of impulsive events.

## ACKNOWLEDGEMENTS

The authors would like to express gratitude to Ashley Crowther and Carrie Janello for the technical assistance provided to this research project, including its documentation.

## REFERENCES

1. D.A. Gilbert, M.F. O'Leary and J.S. Rayce, "Integrating Test and Analytical Methods for the Quantification and Identification of Manual Transmission Driveline Clunk", SAE 2001-01-1502, 2001.

2. R.A. Krenz, "Vehicle Response to Throttle Tip-In/Tip-Out", SAE 850967, 1985.

3. J.W. Biermann and B. Hagerodt, "Investigation of the Clonk Phenomenon in Vehicle Transmissions - Measurement, Modeling and Simulation", Proc. of Inst. of Mech. Eng. Part K: Journal of Multi-body Dynamics, 213, 53-60,1999.

4. M.T. Menday, H. Rahnejat and M. Ebrahimi, "Clonk: an Onomatopoeic Response in Torsional Impact of Automotive Drivelines", Proc. of Inst. of Mech. Eng. Part D: Journal of Automobile Engineering, 213, 349-357, 1999.

5. C.K. Chae, Y.W. Lee, K.M. Won and K.T. Kang, "Experimental Analytical Approach for Identification of Driveline Clunk Source & Transfer Path", SAE CONG-65, 2004.

6. K. Govindswamy, M. Hueser, T. D'Anna, P. Diemer, and C. Roxin, "Study of Low-Frequency Driveline Clunk During Static", SAE2003-01-1480, 2003.

7. B. Volinski, "Methodology: Automatic Transaxle Lash Study for Park Disengagement Clunk", SAE 1999-01-1765.

8. Ph. Couderc, J. Callenaere, J. Der Hagopian and G. Ferraris, "Vehicle Driveline Dynamic Behavior: Experimentation and Simulation", Journal of Sound and Vibration, 104(2), 133-157, 1998.

9. R. Singh, H. Xie and R. J. Comparin, "Analysis of Automotive Neutral Gear Rattle", Journal of Sound and Vibration, 131(2), 177-196, 1989.

10. E.P. Trochon, "Analytical Formulation of Automotive Drivetrain Rattle Problems", M.S. Thesis, The Ohio State University, 1997.

11. T.C. Kim and R. Singh, "Dynamic Interactions between Loaded and Unloaded Gear Pairs under Rattle Conditions", SAE 01NVC-100, 2001.

12. Personal communications with automotive engineers, 2003-2004.

13. A. Crowther, N. Zhang, R. Singh, "Development of a Clunk Simulation Model for a Rear Wheel Drive Vehicle with Automatic Transmission", SAE 2005-01-2991

## CONTACT

Professor Rajendra Singh
Acoustics and Dynamics Laboratory
Center for Automotive Research
The Ohio State University
Email: singh.3@osu.edu
Phone: 614-292-9044
Website: www.AutoNVH.org

| Torsional Mode ($r^{th}$) | Surging Mode ($r=1$) | | Gear Box Mode ($r=2$) | | Clutch Hub Mode ($r=3$) | |
|---|---|---|---|---|---|---|
| Torsional Model | 7-DOF | 19-DOF | 7-DOF | 19-DOF | 7-DOF | 19-DOF |
| Natural Frequency $f_r$ [Hz] | 7.5 | 7.5 | 63.3 | 63.3 | 329.2 | 330.2 |
| Normalized Modal Displacements | | | | | | |
| Engine & Flywheel ($\theta_{EF}$) | 1.000 | 0.998 | -0.059 | -0.057 | -0.002 | -0.003 |
| Clutch Hub ($\theta_C$) | 0.765 | 0.762 | 0.935 | 0.935 | 1.000 | 1.000 |
| Input Shaft + Speed Gears ($\theta_{IS}$) | 0.735 | 0.732 | 1.000 | 0.999 | -0.521 | -0.531 |
| Output Shaft1 + Speed Gears ($\theta_{OS1}$) | 0.734 | 0.731 | 1.000 | 1.000 | -0.553 | -0.562 |
| Output Shaft2 + Speed Gears ($\theta_{OS2}$) | 0.727 | 0.731 | 0.994 | 1.000 | -0.618 | -0.562 |
| Differential ($\theta_{DF}$) | 0.725 | 0.729 | 0.993 | 0.998 | -0.625 | -0.568 |
| Wheels & Vehicle ($\theta_{WV}$) | -0.045 | -0.045 | -0.001 | -0.001 | 0.000 | 0.000 |

Table 1 Comparison of torsional mode shapes and natural frequencies for the 19-DOF and 7-DOF linear models as shown in Figures 2 and 3, respectively.

| Metric | Definition | Expression |
|---|---|---|
| $Q_1$ | Instantaneous speed change at the point of impact | $\Delta\left[\alpha_G\alpha_D\dot{\theta}_{DF}\right]$ |
| $Q_2$ | Peak to peak torsional acceleration value | $\ddot{\theta}_{DF\_P-P}$ |
| $Q_3$ | Peak amplitude of the interfacial torque within a gear pair | $\Delta\left[R_{DF}F_D(x_{rD},x_{bD})\right]$ |
| $Q_4$ | Nature and number of impacts | 0: No impacts<br>S(1): Single-sided impact<br>S(m): multiple single-sided impact<br>D(1): Double-sided impact<br>D(m): Multiple double-sided impacts |

Table 2 Metrics proposed to assess the nature and severity of clunk.

| Torque Type (Figure 9) | $Q_1$ | $Q_2$ | $Q_3$ | $Q_4$ |
|---|---|---|---|---|
| | [rpm] | [rad/s$^2$] | [N-m] | Impact Types |
| A | 65 | 9750 | 194 | D(m) |
| B | 60 | 9100 | 176 | D(m) |
| C | 48 | 7240 | 122 | S(1) |

Table 3 Effect of torque shapes on clunk during the tip-in event.

| Torque Type (Figure 9) | $Q_1$ | $Q_2$ | $Q_3$ | $Q_4$ |
|---|---|---|---|---|
| | [rpm] | [rad/s$^2$] | [N-m] | Impact Types |
| A | 58 | 8800 | 166 | D(m) |
| B | 47 | 6920 | 136 | D(m) |
| C | 33 | 4600 | 91 | 0 |

Table 4 Effect of torque shapes on clunk during the tip-out event.

| $k_{C11}$ (= $k_{C12}$) | $k_{C21}$ (= $k_{C22}$) | $Q_1$ | $Q_2$ | $Q_3$ | $Q_4$ |
|---|---|---|---|---|---|
| [N-m/rad] | [N-m/rad] | [rpm] | [rad/s$^2$] | [N-m] | Impact Types |
| 5 | $\gamma$ | 38 | 5200 | 102 | S(m) |
| 5 | 0.5 $\gamma$ | 37 | 5040 | 101 | S(m) |
| 5 | 2 $\gamma$ | 39 | 5300 | 104 | S(m) |
| 50 | $\gamma$ | 16 | 2320 | 40 | 0 |
| 50 | 0.5 $\gamma$ | 18 | 2636 | 45 | 0 |
| 50 | 2 $\gamma$ | 31 | 3100 | 56 | 0 |

**Table 5** Effects of $k_{C11}$ and $k_{C21}$ on clunk during the tip-out event where $\gamma$ =1800N-m/rad, $\phi_{11}=5$ deg., $\phi_{12}=-5$ deg., and $H_1$= $H_2$=0.